Astron. Astrophys. 327, 1155–1163 (1997)

ASTRONOMY AND ASTROPHYSICS

A numerical simulation of the Wilson-Bappu relationship

Q.-Q. Cheng, O. Engvold, and Ø. Elgarøy

Institute of Theoretical Astrophysics, University of Oslo, PO Box 1029 Blindern, N-0315 Oslo, Norway

Received 26 May 1997 / Accepted 11 July 1997

Abstract. A numerical investigation of Wilson-Bappu relationship for CaII H and K lines in a series of non-active late-type main sequence stars is performed. Atmospheric models are constructed with given effective temperatures and surface gravities using a time-dependent hydrodynamic code. Mechanical heating by acoustic waves is included in the simulations. Radiative energy losses are treated by using tabulated Rosseland mean opacities in the photosphere, solving the transfer equation for the strongest lines in the chromosphere, and assuming optically thin emissivities in the corona.

In the static (time-averaged) atmospheres, we find that the calculated profiles of the CaII K line for different stars show a Wilson-Bappu relationship which is in good agreement with the empirical form. In different stars the lines are formed at an atmospheric height where the column mass density, which is related to the line opacity, is different, and the full width at half maximum of the CaII line emission core broadens as a result of increasing column mass density in the chromosphere. A correct choice of turbulence velocity is important for the calculation of line width in later dwarf stars.

It is well known that stellar atmospheres are dynamic. A more realistic approach is therefore to average line profiles resulting from dynamic atmospheres that represent different instants (phases) of acoustic waves. We find that the time-averaged line profiles in dynamic atmospheres are asymmetric with strong emission on the violet side of the line center. With increasing atmospheric heating the line intensity increases and the base emission line width broadens, while the variation of peak width is not significant.

Key words: hydrodynamics – lines: profiles – star: atmospheres; chromospheres; late-type; fundamental parameters

1. Introduction

The H and K spectral lines of CaII at 3968.5 Å and 3933.7 Å are the only resonance lines of a majority element formed at chromospheric heights which can be accessed by Earth-based telescopes. These lines provide an important tool for the diagnostics of the chromospheres of late-type stars and for theoretical studies of line formation.

The remarkable correlation which was discovered by Wilson and Bappu (1957), shows that the full width at half maximum (FWHM) W_0 of the emission core of the chromospheric CaII H and K lines in late-type stars (effective temperature equal to that of the Sun and cooler) broadens systematically with increasing absolute visual magnitude M_v. This relation is closely obeyed by most cool stars ranging from dwarfs to super giants over 15 magnitudes (Wilson 1959), and for the CaII K line it can be expressed by the empirical formula as (Wilson 1976, Elgarøy et al. 1990):

$$M_v = A \cdot log(W_0) + B, \tag{1}$$

where A and B are constants.

Analogous relations have also been found for the MgII h & k lines and the hydrogen $Ly\alpha$ line (Dupree 1976; Weiler & Oegerle 1979; Vladilo et al. 1987; Elgarøy et al. 1988; Elgarøy et al. 1990).

The Wilson-Bappu relation gives a fundamental link between the total energy emitted by the star and the structure of its chromosphere. The emitted total energy may be determined by global parameters such as the effective temperature $T_{\rm eff}$, the surface gravity g and the metal abundance (Lutz & Pagel 1982). The resonance lines of CaII reflect the temperature structure and the heating in the chromosphere. Thus, investigating the central CaII H and K line profiles for various late-type stars do not only provide information about the absolute stellar magnitudes related to the Wilson-Bappu effect, but may also help us to understand the heating and the structure of the chromospheres. Such understanding is crucial for the explanation of many physical phenomena in stellar atmospheres.

Interpretations of the width/luminosity relations fall into two categories. The first is usually to relate the line width to chromospheric velocity fields caused by turbulence, and subsequently to relate these velocity fields to other fundamental stellar parameters such as luminosity (Hoyle & Wilson 1958; Wilson 1967; Lutz and Pagel 1982). This explanation ignores the complexities of non-LTE line formation. The other approach is to assume

Send offprint requests to: Q.-Q. Cheng

that the chromospheric column mass density, by its relation to the line opacity, is the dominant factor for the Wilson-Bappu effect (Ayres et al. 1973; Ayres & Linsky 1975; Engvold & Rygh 1978; Engvold and Elgarøy 1987). However, a satisfactory theoretical explanation of the Wilson-Bappu effect in detail has not yet been produced.

The profiles and fluxes of chromospheric resonance lines depend on the atmospheric temperature structure. In the calculations of model atmospheres a non-radiative heating is required to balance the energy losses. The chromospheres of cool stars are believed to be heated by two types of mechanisms (Ulmschneider et al. 1991; Schrijver 1995; Peterson and Schrijver 1997), a magnetic mechanism which is correlated with stellar rotation, and an acoustic mechanism which does not depend on rotation and is suspected to be responsible for the minimal emission fluxes observed in the cores of chromospheric strong lines. The heating caused by energy dissipation of acoustic waves is usually called "basal" heating, because theoretical examinations of the fluxes of CaII and MgII emission lines for late-type main sequence stars strongly suggest that the acoustic waves represent the basic heating mechanism (Rutten et al. 1991; Buchholz & Ulmschneider 1994). Acoustic heating is expected to dominate, or even to be the only heating mechanism, in non-active cool stars where dynamo action is not at work (or is operating on a very weak level).

Buchholz and Ulmschneider (1994) computed acoustic wave models of the atmospheres of F, G, K and M main sequence stars, and they found that the CaII and MgII central line emissions are in good agreement with observed values of the chromospheric basal flux limit. Mullan and Cheng (1993, 1994a and 1994b) calculated model atmospheres for M dwarf and F stars, and concluded that acoustic wave heating could be the source of mechanical power for chromospheres and "cool" coronae of the least active late-type stars. These successful numerical simulations suggest that model atmospheres of non-active late-type stars may be derived with acoustic waves as the heating mechanism.

Our investigation is limited to the CaII H and K lines of the least active (non-magnetic) late-type main sequence stars. We first generate the model atmospheres for different stars by using a time-dependent hydrodynamic code, with acoustic wave heating and radiative cooling taken into account. The profiles and fluxes of the CaII emission lines are computed both for time-averaged atmospheric structures and for snapshots of dynamic atmospheres. In the case of the time-averaged model atmospheres, we find a Wilson-Bappu relationship which agrees well with the empirical Eq. (1). The presumed more realistic approach, with instantaneous realizations of dynamic chromospheres, on the other hand, does not give a similarly good agreement with observations.

The paper is structured as follows: Sect. 2 describes the hydrodynamic methods, the computation of the spectral lines, and the generation of modeling atmospheres. Sect. 3 gives the results and discussions. Conclusions are presented in Sect. 4.

2. Methods

2.1. Hydrodynamic computation

In our time-dependent numerical simulations, the hydrodynamics of acoustic wave propagation are followed in detail, and the atmospheric response properties are investigated in order to know the structure of the model atmospheres. A wave train is injected at the lower boundary of the computational domain, and the hydrodynamic equations are integrated to determine how the atmospheric gas responds to the waves.

We solve the time-dependent hydrodynamic equations using an *implicit conservative method* (Mulder & Van Leer 1985; Korevaar & Van Leer 1988; Cheng 1992a; Mullan & Cheng 1993). This method solves the equations of mass, momentum and energy in Euler and conservation form by dividing the space coordinate into slabs and considering the integral values of quantities of state within each slab rather than the values at the center of the slab. The directions of the flow of hydrodynamic information in the calculations are taken into account by flux–vector splitting. Since the information about the variables after a time step is used in the calculations of the solution, the method is stable, large time steps are allowed if the solution approaches a stationary solution, and very non-linear events such as shocks can be treated reasonably well.

It is assumed that the atmosphere is plane parallel. At the bottom of the atmosphere, we introduce acoustic waves generated by a piston. At the top of the atmosphere a transmitting boundary is used in order to ensure that disturbances and/or hydrodynamic information can pass freely through the boundary without reflection (Cheng 1991).

The equations and the numerical method have been described in detail in previous papers (Cheng 1992a; Mullan & Cheng 1993) and these therefore need not to be repeated. The previous papers also outline how to calculate thermal conduction and ionization of hydrogen. The treatment of the radiative loss and the mechanical heating are described below.

2.2. Radiative cooling and acoustic heating

Apparently, in order to understand the propagation and dissipation properties of acoustic waves in the stellar atmospheres, a proper treatment of radiative energy losses is required in the calculations. In our code, radiation losses are treated by different methods at different atmospheric regions (Mullan & Cheng 1993). In the photosphere, we use tables of Rosseland mean opacity computed by Kurucz (1992) and solve the equation of radiative transfer in the continuum to get the net radiative cooling rate. In the chromosphere, the radiative transfer equation is solved (using a core-saturation method) for the strongest lines CaII, MgII and $Ly\alpha$, to represent the total emissions (see also Cheng 1992b). From the atmospheric model calculations for the Sun (Vernazza et al. 1981), it has been shown that the $Ly\alpha$ line loss rate is much larger than the other hydrogen contributions there, and that of $H\alpha$ and the Balmer continuum, one being a cooling and the other a heating mechanism, cancel energetically. Therefore, the net contribution of hydrogen to the radiative loss

is roughly due only to the $Ly\alpha$ line. Ulmschneider et al. (1987) have justified that a scaled $MgII\,k$ line can be used to represent the total radiative loss of the middle chromosphere since its calculated net radiative cooling rate is a substantive fraction of the total at this layer. In the corona, where the temperature is larger than $50,000\,K$, the optically thin approximation (McWhirter et al. 1975) is employed to compute the radiation losses.

In order to get a correct temperature structure of the atmosphere, one needs to consider mechanical heating that balances the radiation losses. Since the heating problem in stellar atmospheres has not yet been solved, as discussed in Sect. 1, we assume that energy deposition of acoustic waves is the heating mechanism for the least active late-type main sequence stars, where magnetic fields are weak or absent. The energy flux and spectrum of acoustic waves generated in the convection zone of stars can be computed theoretically. The most advanced theoretical method to compute acoustic wave generation from the turbulent motions in stellar convection zones has been developed by Stein (1967, 1968). Based on this theory Bohn (1981, 1984) calculated the acoustic wave generation for a series of late-type stars. Stein's theory was recently rediscussed by Musielak et al. (1994) for the Sun. They found that the results by Bohn are basically correct except that, due to somewhat unrealistic assumptions about the spatial and temporal parts of the turbulent energy spectrum, the magnitude of the acoustic wave generation might be overestimated. However, as the extension of Musielak et al.'s work to stars other than the Sun is presently unavailable, and in particular Bohn's basic results remain unchanged, we use Bohn's calculations of the fluxes and spectra of acoustic wave generation and choose a mixing-length parameter $\alpha = 1$ in our numerical simulations.

Bohn's work indicates that there is an important distinction between the acoustic spectrum in a relatively hot main-sequence star (such as F and G star) and the spectrum in a star as cool as an M dwarf. In an F or G star, the acoustic spectrum peaks at a period P_* which is rather short compared to the acoustic cutoff period $P_A = 4\pi c_s/\gamma g$ of the atmosphere: $P_A/P_* = 5-10$. Here c_s is the sound speed, g the gravitational acceleration and $\gamma = 5/3$. However, in an M dwarf star, the acoustic spectrum peaks at relatively longer periods: P_* approaches the cutoff period P_A itself. Since the acoustic spectrum is not monochromatic, but falls off from a maximum at P_* toward smaller values at shorter or longer periods in a star, we prefer not to represent the acoustic spectrum by a monochromatic flux. Waves near the shorter period are more likely to undergo radiative damping and to deposit their energy in the lower part of the atmosphere, while the long-period waves could carry energy to a larger distance and are therefore believed to be more important in the heating of the upper atmosphere. Therefore, based on the above arguments, we will adopt two acoustic wave terms with periods of P_A and $P_A/5$ for our time-dependent calculation of atmospheric models.

2.3. Computation of line profiles

Line profiles and FWHM of CaII are computed using the code MULTI of Carlsson (1986; see also Scharmer & Carlsson 1985).

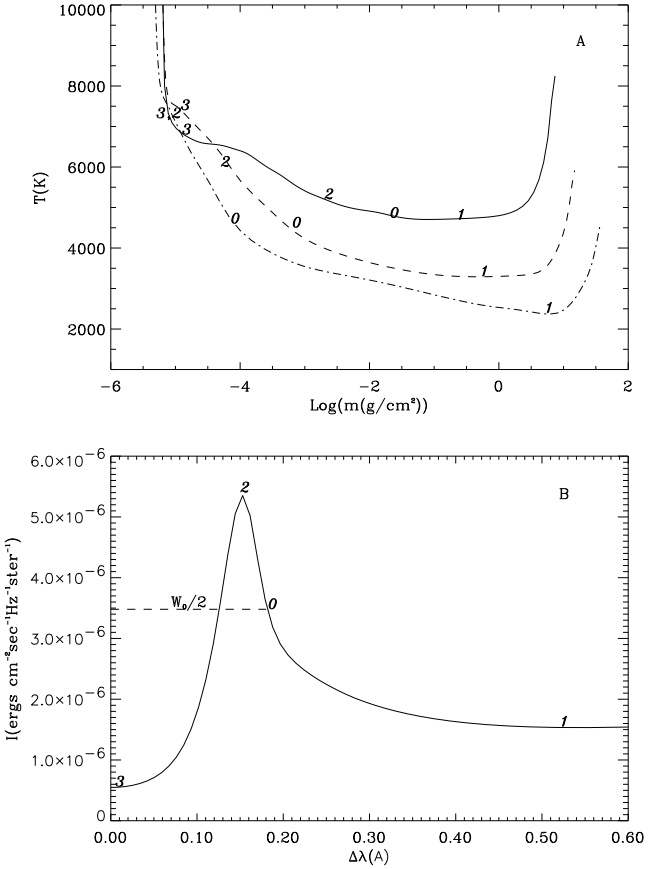

Fig. 1. a Temperature distributions as a function of column mass density $m\,(g\,cm^{-2})$ for the time-averaged atmospheric models. Solid line: $T_{\rm eff} = 5800\,K$ and $g = 2.74 \cdot 10^4\,cm\,s^{-2}$; dashed line: $T_{\rm eff} = 4000\,K$ and $g = 7.0 \cdot 10^4\,cm\,s^{-2}$; chain line: $T_{\rm eff} = 3000\,K$ and $g = 8.66 \cdot 10^4\,cm\,s^{-2}$. **b** Schematic CaII K line profile for a typical late-type star. The numbers 3, 2, 1 and 0 indicate the formation heights (in **a**) of the line where the monochromatic optical depth $\tau(\lambda) = 1$ for the corresponding wavelength at line center, line peak, line minimum, and half maximum where we measure the Wilson-Bappu width W_0 (in **b**)

This program solves the equations of multi-level non-LTE radiative transfer coupled with statistical equilibrium and particle conservation for a plane-parallel geometry using the method developed by Scharmer (1981). In our computation a complete frequency redistribution (CRD) in the scattering process is assumed and a 6-level atom model for single ionized calcium is employed. Background continua are treated in LTE. Microturbulence velocity is set to a constant $4\,km\,s^{-1}$ throughout the atmosphere except when a different value is specified. Since our models deal only with main sequence stars, solar abundances have been chosen.

2.4. Modeling procedure

In the present paper, we adopt a fully time-dependent hydrodynamic approach where the acoustic waves are explicitly computed. Starting with a given effective temperature $T_{\rm eff}$ and grav-

itational acceleration g at the surface of a star, we prescribe an initial guess of the temperature distribution in all zones of the atmosphere: this is typically close to a gray model in the lower atmosphere and rises steeply to high values of the corona. Then, the system of equations is integrated forward in time, with the radiation, ionization, conduction and mechanical heating taken into account. At the bottom boundary (the height $x = 0$) of our computational domain, we assume a temperature $T = T_{\rm eff}$ and choose a pressure where the optical depth $\tau_{5000} = 1$. To power this initial profile, we inject acoustic waves with specified periods and velocities (fluxes) into the atmosphere at the lower boundary. This velocity perturbation behaves like a "piston" and continues to work for as long as the calculation runs. The acoustic waves propagate upward through the atmosphere and deposit heat as they evolve nonlinearly.

At first, large velocities upward and downward are induced by the spuriously located temperature ramp, and these may persist for long times (many sound crossing times) if the pressure at the upper boundary is not chosen correctly. Iterating on the choice of the pressure at the upper boundary, the temperature structure adjusts itself such that, after typically about ten thousands seconds, time-averaged local deposition of mechanical energy is (nearly) balanced by radiative and conductive losses in a physically consistent manner. When this occurs, we then determine the atmospheric structure (such as the temperature and pressure distributions) by averaging over the last several wave periods of the simulation. Fig. 1a shows the time-averaged temperature structure as a function of mass column density (m) for three model atmospheres, with a solid line for the star of effective temperature $T_{\rm eff} = 5800\,K$ and gravity $g = 2.74 \cdot 10^4\,(cm\,{\rm s}^{-2})$, dashed line $T_{\rm eff} = 4000\,K$ and gravity $g = 7.0 \cdot 10^4\,(cm\,{\rm s}^{-2})$, and chain line $T_{\rm eff} = 3000\,K$ and gravity $g = 8.66 \cdot 10^4\,(cm\,{\rm s}^{-2})$. Further explanations of this Figure will be given below (Sect. 3.1). It should be noted that our atmospheric models include a chromosphere-corona transition region, which may play a fundamental role for the dynamics of the upper chromosphere and for the computation of emission lines. The location of temperature minimum is also successfully reproduced. In this paper, however, the coronal portion of the models is of interest mainly as a supplier of heat conduction to the transition region to provide a reasonable temperature structure.

Once a time-averaged atmosphere is obtained, one computes the widths and profiles of the CaII H and K lines and studies the relations between the stellar parameters and line widths. For comparison and for explaining the line asymmetry of observations, the line profiles are also calculated with specified instantaneous atmospheres, and then a time average of the line profiles is made.

3. Results

In this Section the numerical results of model atmospheres and CaII line profiles will be discussed. The related data concerning stars, such as the effective temperatures ($T_{\rm eff}$), surface gravities (g) and absolute visual magnitudes (M_v) as well as the assumed turbulence velocities (v_{turb}), are listed in Table 1. Since we have limited information about the turbulent velocity fields in stellar atmospheres, for the computation of CaII lines, the turbulent velocities in the line formation layers are assumed to be a constant of $v_{turb} = 4\,{\rm km\,s}^{-1}$. In order to make a comparison we also studied one case with $v_{turb} = 1\,{\rm km\,s}^{-1}$.

3.1. Time-averaged atmospheres

The time-averaged atmospheres (mean temperature and mass density distributions) are used to compute line profiles and widths. Fig. 2 shows the line profiles of the CaII K lines computed with the three model atmospheres given in Fig. 1a. Where $I\,(erg\,cm^{-2}\,sec^{-1}\,Hz^{-1}\,ster^{-1})$ is the intensity and $\Delta\lambda\,(\text{Å})$ the wavelength displacement from line-center. The line profiles at the right hand side of the Figure are the same as those at the left side but show only the emission cores. It is clearly seen that the line profiles are symmetric and that the line width becomes narrower towards later type (smaller mass) of main sequence stars. In the coolest star where $T_{\rm eff} = 3000\,K$, the separation of wave length (λ) between blue peak and red peak becomes too small to be recognized. It is also found that the brightest emission lines (largest intensity) are associated with the largest widths, which implies that the broadening is actually an effect of opacity of the line.

Table 1 summarizes the result of the calculations. $W_0\,({\rm km\,s}^{-1})$ is the full width at half maximum of the emission lines, W_0^* is the expected result from the empirical form $M_v = -14.94 \cdot log(W_0^*) + 27.59$ given by Wilson (1976) for the K lines, and $F\,({\rm ergs}\,cm^{-2}\,{\rm s}^{-1})$ is the radiative energy flux. T is the temperature and m the mass column density where the monochromatic optical depth $\tau(\lambda) = 1$ for the corresponding wave length of the K line as shown in Fig. 1b (where the number 3 indicates the line center, 2 the emission peak, 1 the minimum point between core and wing, and 0 the position of half maximum where we measure the Wilson-Bappu width W_0. The objective for the calculation of the temperature and mass density at $\tau(\lambda) = 1$ is to make a comparison of atmospheric structures where the line features supposedly originate.

For a comparison, the lines resulting from the VAL model atmosphere C of the Sun given by Vernazza et al. (1981) are also computed in Table 1. One finds that the difference between the result for the VAL model and that for our acoustic heating atmosphere with $T_{\rm eff} = 5800\,K$ is small. For the calculation of $T_{\rm eff} = 4000\,K$ a small increase of gravity does not produce a significant effect on the result. When the turbulent velocity is kept at constant $4\,{\rm km\,s}^{-1}$ in the computation of lines, Table 1 shows a Wilson-Bappu relationship between the line width W_0 and the absolute visual magnitude M_v. It is clearly seen that the widths and fluxes of the CaII H and K lines both increase with increasing absolute magnitude of stars. This is due to the fact that the line opacity, being proportional to the column mass density, increases in the earlier type stars (more explanations will be found below). However, comparing the calculated K line widths with the expected widths W_0^* from the empirical form, we find that the line widths are narrower than the expected value for the

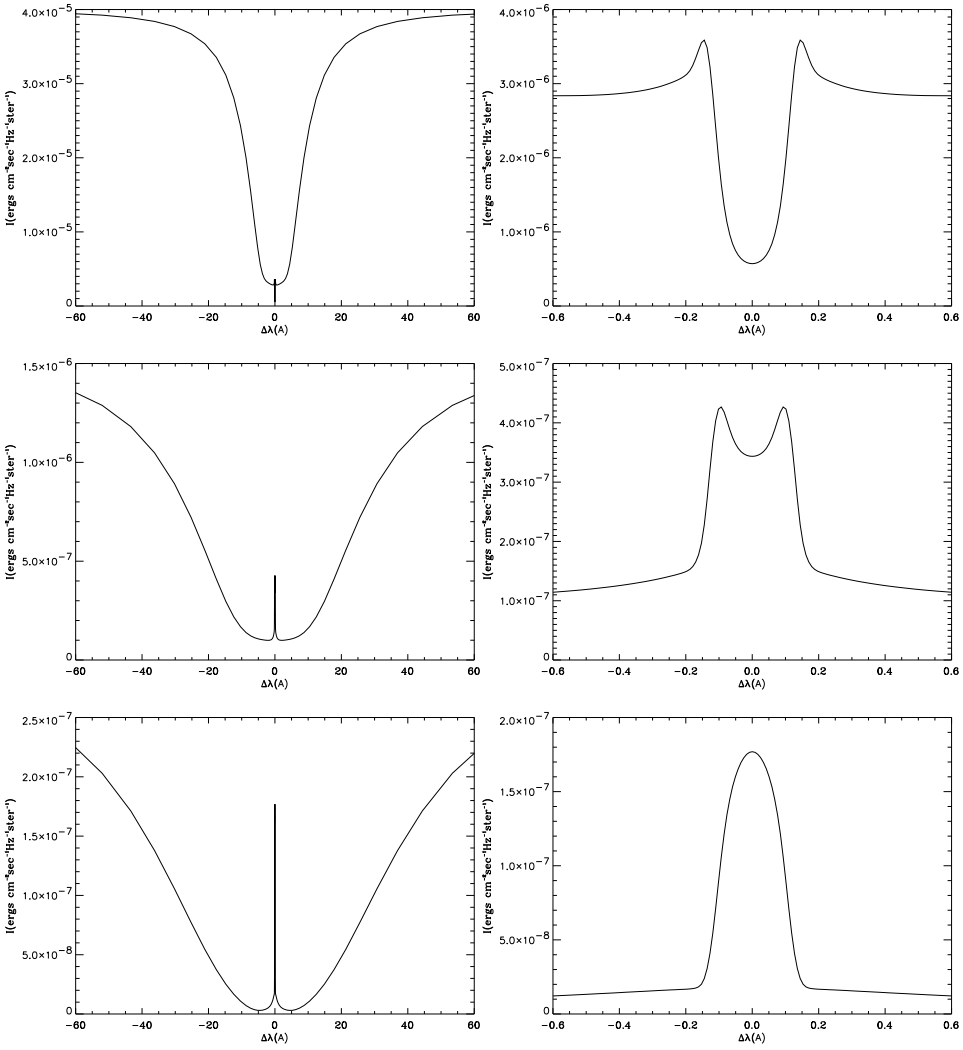

Fig. 2. Calculated K line profiles for the time-averaged atmospheres with $T_{\rm eff}$ = 5800 K (upper diagrams), $T_{\rm eff}$ = 4000 K (middle), and $T_{\rm eff}$ = 3000 K (lower). Left side shows the full view while right side only the emission core

Table 1. Summarized results with time-averaged atmospheres

		Stars		H line	K line						
T_{eff} (K)	$log(g)$ ($cm\ s^{-2}$)	M_v	v_{turb} ($km\ s^{-1}$)	$W_o(H)$ ($km\ s^{-1}$)	$W_0(K)$ ($km\ s^{-1}$)	$W_0^*(K)$ ($km\ s^{-1}$)	$F(K)$ ($erg\ cm^{-2}\ s^{-1}$)	$log(m_3)$ ($g\ cm^{-2}$)	$log(m_2)$ ($g\ cm^{-2}$)	$log(m_0)$ ($g\ cm^{-2}$)	T_0 (K)
Sun(VAL)	4.44	4.80	4.0	27.03	30.01	33.53	$6.2 \cdot 10^5$	−5.0	−2.6	−1.7	4420
5800	4.44	4.80	4.0	27.86	30.59	33.53	$8.8 \cdot 10^5$	−4.9	−2.7	−1.7	4800
4000	4.44	8.20	4.0	20.28	21.62	19.85	$6.9 \cdot 10^4$	−4.9	−4.3	−3.2	4650
4000	4.85	8.20	4.0	20.39	21.34	19.85	$5.6 \cdot 10^4$	−4.9	−4.3	−3.2	4600
3000	4.94	13.8	4.0	14.59	15.65	8.37	$5.4 \cdot 10^3$	−5.1	−5.1	−4.3	4700
3000	4.94	13.8	1.0	7.19	7.77	8.37	$4.4 \cdot 10^3$	−5.2	−5.2	−4.4	4700

star with $T_{\rm eff}$ = 5800 K, but somewhat larger for cooler stars, especially with $T_{\rm eff}$ = 3000 K. There are several possibilities which may be responsible for this deviation from the empirical slope of the Wilson-Bappu relation. First, a single value of turbulent velocity has been used in the calculations for all the stars. According to Scharmer (1976), the chromospheric turbulent velocity may be proportional to the effective temperature ($T_{\rm eff}$). The turbulent velocity fields for stellar chromospheres are supposed also to vary with height. Thus, a corresponding turbulent velocity should be identified for different stars. For example, when v_{turb} is reduced to 1 km s^{-1} for the calculation with $T_{\rm eff}$ = 3000 K, we found in fact that the K line width W_0 decreases to 7.77 km s^{-1}. This value is in good agreement with the predicted width of 8.37 km s^{-1} by the empirical form. Second, the CRD assumption for the scattering process may have an effect on the computation of line profiles. The coherent nature of

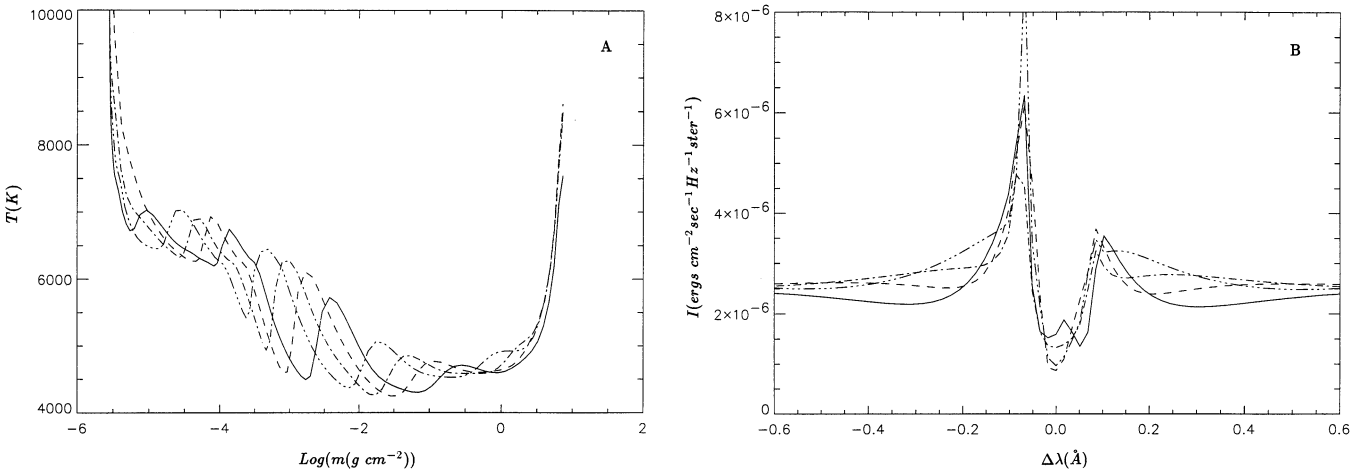

Fig. 3a and b. Temperature distributions as a function of column mass density (left diagram) and the corresponding CaII K line profiles (right diagram) for the dynamic modeling atmosphere with $T_{\rm eff}$ = 5800 K. The display starts at an arbitrarily chosen time and is at 4 different times with time interval of 12 seconds (plotted with solid, dashed, chain and point lines, respectively)

partial redistribution (PRD) reduces the net escape probability of photons from the line core to the wings, and hence the line width could be reduced. Including PRD is a task for future studies. Third, for the coolest stars, the chromospheres may contain a larger fraction of neutral Calcium, and then the density of single ionized Calcium could be effectively reduced. This leads to an optically thinner case in which the line becomes narrower.

In order to examine the dependence of the line profiles on the structure of stellar atmospheres, we have calculated the temperatures and column mass densities at the heights where the monochromatic optical depth of the K lines $\tau(\lambda)$ = 1 for specified wave length at line center (represented by number 3), peak (number 2), minimum (number 1) and half maximum (number 0) (see Figure 1). Checking on the Table 1 and Fig. 1, we found that the line centers are formed at the top of the chromospheres where the column mass densities (m_3) have almost the same value for all the concerned stars. However, the line peaks are formed at the upper layer of the chromospheres where the column mass density (m_2) decreases quickly towards cooler stars. It is interesting to see that the half maxima of the emission cores, where we measure the FWHM W_0, originate from the chromospheric heights where the temperatures (T_0) are around $4700K$ but the column mass densities m_0 are very different, with higher column mass density for earlier type stars. Noticing the fact that the lines with larger width (W_0) are formed at higher column mass density in the chromospheres, a conclusion can be drawn here that the line profile strongly depends on the atmospheric structure in the line formation height: i.e. on the variation of temperature with height, and on the line opacity which increases with increasing column mass density. It is the variation of column mass density of the atmospheres of stars of different luminosity that causes the Wilson-Bappu effect, if the turbulent velocity is assumed to have a constant value. Our simulated result also shows that the stellar chromospheres are thicker in stars with low gravity and high effective temperature, which is consistent with the suggestion by Ayres (1979).

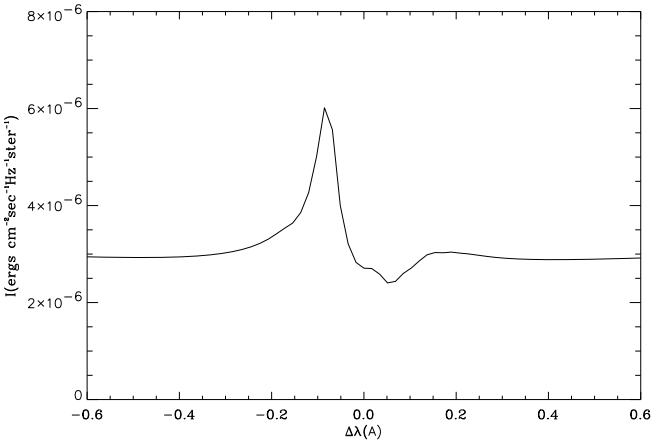

Fig. 4. Time average of the calculated K line profiles for the dynamic atmosphere with $T_{\rm eff}$ = 5800 K

3.2. Instantaneous dynamic atmospheres

In a realistic situation, stellar atmospheres are dynamic and material motions and shocks are present. Shocks produce a steep velocity and temperature gradient, and may have a strong effect on the generation of the lines. It is important to compare the physics in the instantaneous dynamic situation with the conclusions we have drawn from the analysis of the time-averaged atmospheres. In this Section we show the atmospheric structures and the line profiles of a dynamic simulation with effective temperature $T_{\rm eff}$ = 5800 K, and discuss the obtained results.

Fig. 3a (left diagram) displays the temperature distributions as a function of column mass density in the instantaneous dynamic atmosphere. The plot shows the situation at 4 different times with time intervals of 12 seconds, and starts at an arbitrarily chosen time (solid line). It is clearly seen that the waves propagate upwards in the atmosphere and a large variation of

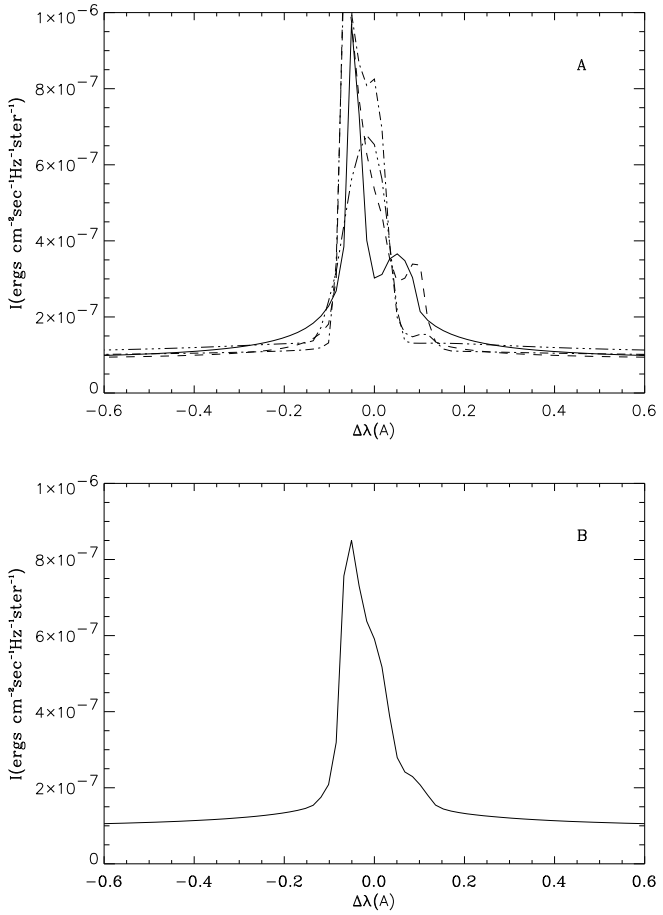

Fig. 5. a CaII K line profiles from the dynamic atmosphere of $T_{\rm eff}$ = 4000 K at 4 different times (solid, dashed, chain and point lines, respectively), with time interval of 10 seconds and starting at an arbitrarily chosen time. **b** Time average of the K line profiles from the dynamic atmosphere of $T_{\rm eff}$ = 4000 K.

the temperature gradient is present. There are strong shocks in the area where the emission cores of the CaII lines are formed.

The line profiles using the atmospheric structures given in Fig. 3a (left diagram) have been computed. The corresponding K line intensities, as a function of wavelength displacement $\Delta\lambda$ from the line center, are shown in Fig. 3b (right diagram). Fig. 4 shows the time average of the K line profiles over a few acoustic wave periods for the dynamic atmosphere. Comparing Fig. 3b (right diagram) and Fig. 4 with Fig. 2 (upper diagram), we find that the behavior of the line is now quite different from that computed with the time-averaged atmosphere, although the line width varies only slightly. The line profiles are now asymmetric with strong emission on the violet side of the line center and rarely any emission on the red side. This asymmetry is a hydrodynamic phenomenon that can be explained by the correlation between velocity and temperature structure. Observations of solar CaII H_{2v} and K_{2v} bright grains, which provide important diagnostics of the dynamic interaction between the photosphere and the chromosphere in the interiors of network cells, confirm this asymmetric behaviour.

The reason for this asymmetry of the line profiles has been attributed to the material motions within the stellar atmospheres (Rutten & Uitenbroek 1991; Rammacher & Ulmschneider 1992). In their recent theoretical study of the formation of Solar CaII H and K bright grains, Carlsson and Stein (1992, 1997) gave a detailed explanation of the line asymmetry. They found that the asymmetry of the line profiles is produced by the large velocity gradients existing near the chromospheric height of 1 Mm. Material motion Doppler shifts the frequency to the blue side behind the shocks where the velocity is positive (upward motion). Shocks propagate generally into downflowing material, so there is little matter above to absorb the Doppler shifted radiation. The corresponding red peak is absent because of the small opacity at the source function maximum and the large optical depth due to overlying material where the radiation is absorbed. Downward motion of the layer where the line center is formed at the top of the chromosphere Doppler shifts the line center to the red side and may also cause absence of the red peak emission (Rutten & Uitenbroek 1991).

Fig. 5a shows the instantaneous K line profiles at 4 different times and Fig. 5b shows the time average of the line profiles over 10 acoustic wave periods for the calculation of the dynamic atmosphere with $T_{\rm eff}$ = 4000 K. It is found again that the line profile varies with time and that it is asymmetric with much stronger emission on the violet side.

In summary, the asymmetric property of the CaII line profiles is common in the realistic dynamic atmospheres. It may indicate that there are more upward propagating shock waves in the stellar chromospheres and that hydrodynamic phenomena are important in the region where the emission originates.

3.3. Line profiles and atmospheric heating

It is of interest to examine the link between the line profiles and chromospheric heating. From theoretical convection zone calculations Bohn (1984) found that the acoustic energy fluxes F (ergs/cm^2/s) are quite sensitive to the choice of the mixing-length parameter α, as they are directly proportional to $\alpha^{2.8}$. Although the correct value to choose for α is not known, values of α between 1 and 2 lead to an uncertainty in the predicted mechanical energy fluxes by factors of up to 7. From Bohn's figures, we derive the mechanical energy fluxes $F = 1.2 \cdot 10^8$ and $3.7 \cdot 10^8$ ergs cm^{-2} s^{-1} for the Sun using α = 1.0 and 1.5, respectively. Moreover, the use of a Lighthill method to compute acoustic fluxes as done by Bohn may not be reliable in the presence of radiative losses: the latter can drive acoustic modes overstable in the convection zone and may lead to significantly larger acoustic fluxes than previously believed possible (Hossain & Mullan 1993). Inclusion of molecules into the opacity and equation of state may also lead to a change in the acoustic energy flux generation in convection zone models. Because of these uncertainties, we consider it worthwhile to explore cases where different incident energy fluxes are used in the modeling calculations.

In order to examine the dependence of calculated atmospheric models and line profiles on the strength of incident

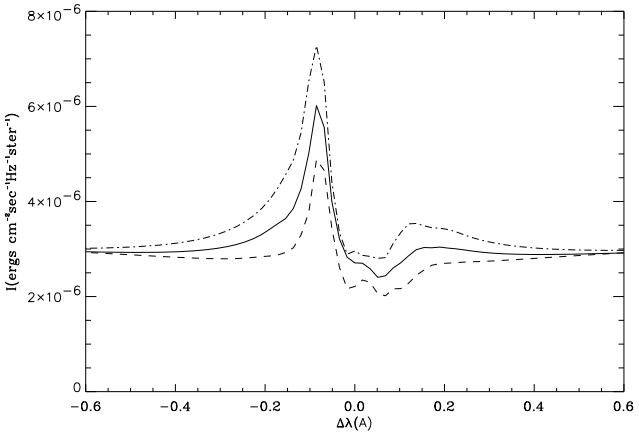

Fig. 6. Same as in Fig. 4 but using three different values of the incident energy flux F (ergs $cm^{-2}\,s^{-1}$) for mechanical heating. Solid line: $F = F_0 = 1.0 \cdot 10^8$; dashed line: $F = F_0/3$; and chain line: $F = 3F_0$

energy for mechanical heating, we have performed three simulations for the model with $T_{\rm eff} = 5800\,(K)$ and $g = 2.74 \cdot 10^4\,(cm\,s^{-2})$, using incident energy fluxes of F_0 $(= 1.0 \cdot 10^8\,erg\,cm^{-2}\,s^{-1})$, $F_0/3$ and $3F_0$, respectively. A time average is made for the instantaneous K line profiles in a dynamic atmosphere. The results are displayed in Fig. 6. It is found that a larger heating in the atmosphere will lead to a stronger emission in the line core and an increased line width. However, it should be noted that whereas the K_1 minimum separation (W_1) broadens with increasing incident mechanical energy flux, the K_2 peak separation (W_2) shows almost no changes. This occurs because in a given star the chromospheric temperature increases and the temperature inversion layer moves deeper into the photosphere if the chromospheric heating is increased. The effect is apparent when chromospheric models for an average quiet region on the Sun and for a very bright network element are compared (Vernazza et al. 1981).

Increasing the chromospheric temperature leads to a rise of the mean electron density and to an enhanced line emission. According to Ayres et al. (1975), the K_1 minima are formed in the Lorentzian damping wing of the line. The width W_1 increases with heating because the chromospheric temperature inversion layer moves deeper into the photosphere where the column mass density and thus the opacity is larger. But the width W_2 should become smaller if the K_2 maxima are also formed in the damping wings (Ayres 1979). This occurs because the increased chromospheric electron density associated with increased heating produces line peaks closer to the line center since the line source function thermalizes in the chromosphere at smaller optical depths of the line center. However, the Doppler core feature of the line dominantly controls the behavior of the line core, producing a broadening of the emission core with increased heating in the layer of the chromosphere where the emission width should be determined by spatially and temporally averaged velocity fields. In consequence, the variation of the width of the peak is insignificant. The Wilson-Bappu width W_0 is intermediate between that of the base emission width and the peak width. Therefore, the width W_0 should show a behavior that is between that of W_1 and W_2.

These predictions might eventually be tested by examining high-resolution CaII H & K profiles from a large sample of late-type stars having similar effective temperatures and surface gravities but different total chromospheric heating. The line core should become brighter and the base emission width should broaden but the peak width should be no significant change when the chromosphere of a star is more active.

This paper addresses only basal flux stars, but all stars fulfill the W-B relation. Activity in non-basal stars seems to be associated with magnetic field. Increasing stellar activity level will lead to an increase of the line emission strength. However, the W-B line width W_0 is insensitive to the emission strength (see also Glebocki and Stawikowski 1978). Hammer (1987) discussed the reason of this insensitivity and suggested that it might be due to "the fact that increasing activity is caused by an increasing number of similar flux tubes: the physics of each tube, and in particular the associated nonthermal motions, are constant for a given type of star (i.e., given $T_{\rm eff}$ and g)". Detailed discussion on active stars is beyond the purpose of this Paper.

4. Conclusions

Using a time-dependent numerical method, we have constructed atmospheric models for a number of non-active late-type main-sequence stars, and investigated the Wilson-Bappu relationship for CaII H and K lines.

In hydrodynamic calculations, the radiative energy losses are treated by different methods at different regions, and the atmospheres are continuously being heated at all times by acoustic waves which are created in the convection zone and subsequently injected at the bottom boundary of our computational domain. In order to extract the mean model atmospheres, averages of physical parameters such as temperature and column mass density over time were taken.

Based on time-averaged model atmospheres, we have computed the line profiles and fluxes of CaII H and K lines and studied their dependence on the atmospheric structures as well as the fundamental parameters of stars. We found that brighter emission lines (larger fluxes) are associated with larger widths, and that the line width becomes narrower towards later type star. Our results confirmed the Wilson-Bappu relation between the full width at half maximum of the emission core of CaII lines and the absolute visual magnitude of stars.

The Wilson-Bappu relationship appears to be a combined effect of column mass density and turbulence velocity. In this work, the column mass density of the chromospheres, which relates to the line opacity, is the main cause of the Wilson-Bappu effect. This is due to the fact that, because the temperature structure varies from one star to another star, the line peaks and half maxima are formed at a chromospheric height corresponding to different column mass density. When examining the calculated results in detail it is found that the line width broadens if the column mass density increases in the chromospheres. It is

noted that the chromospheres are thicker in low-gravity, high-effective-temperature stars.

Stellar atmospheres are dynamic. CaII K line profiles have been calculated with instantaneous dynamic atmospheres, and the results show that a time average of line profiles becomes asymmetric with strong emission on the violet side of the line center. The present results indicate that upward-propagating shock waves are existing in the atmospheres and hydrodynamic phenomena are important in the region where the lines originate.

One notices that the time-averaged atmosphere model gives very different results as compared to the line profile derived from the dynamic atmosphere (average of many profiles). We believe that the latter is more realistic and represents the correct direction to compute line profiles, in spite of the fact that it presently gives poor agreement with observations (calculated asymmetry is much stronger than the observed).

It is stressed that only acoustic waves are used here to heat the atmospheres and, the calculated chromospheric CaII H and K lines represent the non-magnetic, "basal" radiation. The strong asymmetric feature of the line profiles reflects the fact that there are large hydrodynamic motions in the atmosphere. Therefore, it is expected that simulations with magnetic heating mechanism in addition taken into account, will weaken the present strong asymmetry (blue peak relative to red peak) and perhaps give better agreement with observations.

The theoretical study presented in this paper is part of an ongoing program. More work needs to be done in the future for active stars, for giants and super-giants, and for other lines such as MgII. The computation of line profiles may also be improved by including partially coherent scattering (PRD).

Acknowledgements. We would like to thank the referee, R. Hammer, for valuable comments. We are grateful to Mats Carlsson for allowing us to use his radiative code MULTI and for helpful discussions.

References

Ayres T.R., 1979, ApJ 228, 509
Ayres T.R., Linsky J.L., 1975, ApJ 200, 660
Ayres T.R., Linsky J.L., Shine R.A., Chipman E., 1973, Bull. Am. Astron. Soc., 5, 364
Bohn H.U., 1981, Ph. D. thesis, Univ. of Würzburg, Germany
Bohn H.U., 1984, A&A 136, 338
Buchholz B., Ulmschneider P., 1994, in Proc. 8th Cambridge Workshop on Cool Stars, Stellar Systems and the Sun, Ed. J.P. Caillault, ASP Conf. Series
Carlsson M., 1986, Uppsala Astronomical Observatory No. 33
Carlsson M., Stein R.F., 1992, ApJ 397, L59
Carlsson M., Stein R.F., 1997, ApJ 481
Cheng Q.Q., 1991, Ph.D. Thesis, Universität Heidelberg
Cheng Q.Q., 1992a, A&A 266, 537
Cheng Q.Q., 1992b, A&A 266, 549
Dupree A.K., 1976, in Physique des Mouvements dans les Atmospheres Stellaires, eds. R. Cayrel and M. Steinberg (Paris: CNRS), p.439
Elgarøy Ø., Engvold O., Carlsson M., 1990, A&A 234, 308
Elgarøy Ø. et al., 1988, A&A 193, 211
Engvold O., Elgarøy Ø., 1987, in Proc. Fifth Cambridge Workshop on Cool Stars, Stellar Systems and the Sun, Boulder, Colorado, eds. J.L. Linsky, R.E. Stencel, Lect. Notes Phys., 291, 315
Engvold O., Rygh B.O., 1978, A&A 70, 399
Glebocki R., Stawikowski A., 1978, A&A 68, 69
Hammer R., 1987, in Solar and Stellar Physics (5th European Solar Meeting, Titisee), eds. E. H. Schröter and M. Schüssler, Springer
Hossain M., Mullan D.J., 1993, ApJ 416, 733
Hoyle F., Wilson O.C., 1958, ApJ 128, 604
Korevaar P., Van Leer B., 1988, A&A 200, 153
Kurucz R., 1992, private communication
Lutz T.E., Pagel B.E.J., 1982, Monthly Notices Roy. Astron. Soc., 199, 1101
McWhirter R.W.P., Thonemann P.C., Wilson R., 1975, A&A 40, 63
Mulder W.A., Van Leer B., 1985, J. Comput. Phys., 59, 232
Mullan D.J., Cheng Q.Q., 1993, ApJ 412, 312
Mullan D.J., Cheng Q.Q., 1994a, ApJ 420, 392
Mullan D.J., Cheng Q.Q., 1994b, ApJ 435, 335
Musielak Z.E., Rosner R., Stein R.F., Ulmschneider P., 1994, ApJ 423, 474
Peterson R.C., Schrijver C.J., 1997, ApJ 480, L47
Rammacher W., Ulmschneider P., 1992, A&A 253, 586
Rutten R.G.M., Schrijver C.J., Lemmens A.F.P., Zwaan C., 1991, A&A 252, 203
Rutten R.J., Uitenbroek H., 1991, Solar Phys., 134, 15
Scharmer G.B., 1976, A&A 53, 341
Scharmer G.B., 1981, ApJ 249, 720
Scharmer G.B., Carlsson M., 1985, J. Comp. Phys., 59, 56
Schrijver C.J., 1995, A&A Rev. 6, 181
Stein R.F., 1967, Solar Phys., 2, 385
Stein R.F., 1968, ApJ 2, 385
Ulmschneider P., Muchmore, D., Kalkofen W., 1987, A&A 177, 292
Ulmschneider P., Priest E.R., Rosner R. (eds.), 1991, Mechanisms of Chromospheric and Coronal Heating, Springer-Verlag, Berlin
Vernazza J.E., Avrett E.H., Loeser R., 1981, ApJS 45, 635
Vladilo G., Molaro P., Crivellari L., Foing B.H., Beckman J.E., Genova R., 1987, A&A 185, 233
Weiler E.J., Oegerle W.R., 1979, ApJ Suppl. 39, 537
Wilson O.C., 1959, ApJ 130, 499
Wilson O.C., 1967, PASP 79,46
Wilson O.C., 1976, ApJ 205, 823
Wilson O.C., Bappu M.K.V., 1957, ApJ 125, 661

This article was processed by the author using Springer-Verlag LaTeX A&A style file *L-AA* version 3.